A comparative view of alkaline and alkaline-earth elements intercalation into perovskite-type $A_xLa_yTiO_3$ (A = Li, Na, or Mg) based on theoretical calculations and experiments

Carlos Pérez-Vicente, Alejandro Medina, Ricardo Alcántara.*

Departamento de Química Inorgánica e Ingeniería Química, Instituto Químico para la Energía y el Medioambiente (IQUEMA), Facultad de Ciencias, Universidad de Córdoba, Campus de Rabanales, Edificio Marie Curie, E-14071 Córdoba, Spain.

*Corresponding: e-mail: ralcantara@uco.es

Telephone: (+34) 957218568.

ABSTRACT. Perovskite-type titanates are candidates as solid-state electrolyte for alkali metal-ion batteries, although the composition, synthesis temperature, microstructure, and cationic disorder influence on their ionic conductivity, and all of that must be optimized. On the other hand, it is less known that perovskite-type lithium lanthanum titanate is interesting as electrode material for lithium batteries. The reversible capacity is strongly affected by the ions distribution. Having this in mind, we have evaluated titanate perovskites $A_xLa_yTiO_3$, with A = Li, Na and $(x+y) \leq 1$, as electrode active material for lithium, sodium and magnesium batteries. We discuss whether the structure has available sites for further intercalation of univalent (lithium and sodium) and divalent (magnesium) cations. Using both theoretical calculations and experimental results, it is concluded and justified that $A_xLa_yTiO_3$ is very suitable as electrode for lithium battery at room temperature, but not for sodium and magnesium batteries.

Keywords: lithium batteries, sodium batteries, magnesium batteries, $Li_{0.5}La_{0.5}TiO_3$, first-principles computation, ionic conductivity

1. INTRODUCTION

The development of new lithium-ion and post-lithium batteries is an urgent need for the modern society. For that goal, one of the main strategies is to select the most suitable materials for high-performance batteries. For example, the high stability of certain crystal structures can help to develop new electrodes sustaining many charge/discharge cycles. Among the post-lithium batteries, sodium-ion and magnesium-ion batteries are particularly promising.

Since the perovskite structure is very robust, it is worthy to study the intercalation of univalent (proton, lithium, sodium…) and divalent (calcium, magnesium…) cations into its framework. The perovskites with general stochiometry ABX_3 are a large family of compounds with a wide variety of fascinating properties and ease of preparation, and which also could be used in next generation batteries [1]. The framework of the perovskite class is built up of BX_6 corner-sharing octahedra, with the A cation occupying every hole created by 8 BX_6 and in 12-fold cuboctahedral coordination, although the coordination numbers can be reduced in distorted versions of this structure. One could think that the A hole of the perovskite is too large for being occupied by lithium, but the fact is that some perovskites contain lithium and other larger cation in the A sites. In fact, the interesting structure and properties of the perovskites have driven to several research groups to propose this family of compounds as electrode and solid electrolyte.

Perovskite-type lithium lanthanum titanate $Li_{0.5}La_{0.5}TiO_3$ (LLTO) and structurally-related sodium lanthanum titanate $Na_{0.5}La_{0.5}TiO_3$ (NLTO) are being studied as potential solid electrolytes for solid state batteries which would be advantageous in terms of safety compared to batteries based on liquid electrolytes [2-10]. It was found that LLTO is much more promising than NLTO, for a similar structure with space group P4/mmm [10]. Lanthanum ions are a main contribution for the stabilization of the crystalline structure, while lithium ions are the charge carriers, and the

La-layers can block the diffusion of the mobile ions. The degree of ordering/disordering of lanthanum, vacancies and alkali metal ions, and the concentration of Li/La strongly influence on the ionic transport. In fact, the lithium mobility in LLTO can be outstanding [11], and the theoretically calculated value for the bulk ionic conductivity is 3.4×10^{-4} S cm^{-1} [12]. In addition, LLTO becomes a much better electronic conductor at high levels of Li insertion (below 1.5 V vs. Li^+/Li) due to the concomitant reduction of titanium ions from Ti^{4+} to Ti^{3+} [13].

Reversible intercalation of lithium into perovskites, such as praseodymium bismuth lithium titanate [14] and LLTO has been previously reported [15-17]. Thus, LLTO is a promising family of electrode active materials for lithium batteries [17-19]. The good lithium mobility and the framework stability are the main advantages of $Li_{0.5}La_{0.5}TiO_3$ [18]. $Li_{0.1}La_{0.3}NbO_3$ and $La_{1/3}NbO_3$ with A-site deficient perovskite structure are good electrode materials for LIB with zero-strain [20]. Mn-based perovskites also have been studied as negative electrode for lithium-ion batteries [21, 22]. Nanostructured $HoFeO_3$ perovskite, with orthorhombic structure, exhibits very good electrochemical properties in lithium-ion batteries, including high capacity (437 mAh g^{-1}), good cyclability, and excellent rate performance [23].

Since the perovskite-structure is very stable, $LaMnO_3$ has been used to form an epitaxially-grown layer on the surface of layered-Li_2MnO_3 particles which protects the surface of the cathode, and it suppresses the anion activity (O^{2-}, O_2^{2-}) [24]. The antiperovskite-type Li_2TMChO (TM = Mn, Fe, Co, and Ch = S, Se, Te) have been also demonstrated to be useful as cathode for LIB [25, 26]. For Li_2FeSO, theoretically up to 2 Li per formula could be deintercalated. However, the voltage of the Fe^{2+}/Fe^{3+} redox couple is low for a cathode and the DFT calculations found that this material is structurally unstable.

Besides lithium, and within the context of post-Li batteries, batteries based on divalent ions, such as calcium and magnesium, could be an alternative to batteries based on univalent ions, such as lithium and sodium. Thus, the perovskite-type $NaMnF_3$, $NaFeF_3$ and $Na_{0.5}Bi_{0.5}TiO_3$ compounds have been found to be promising as electrodes for sodium-ion batteries [27, 28]. However, finding host materials for reversible accommodation of divalent ions is particularly difficult. First principles calculations found that the energy barrier for Ca-diffusion in perovskite-type $CaMO_3$ (M= Mo, Cr, Mn, Fe, Co and Ni) is too large for practical Ca-ion batteries [29]. Lead-based perovskites ($PbTiO_3$ and $PbZrO_3$) have been used as electrode for M-ion batteries (M = Li, Na, K), and mechanism of the discharge process is a conversion-alloying reaction [30].

Intercalation and diffusion of magnesium into perovskites have been little explored. A prototype quasi-solid-state MIB with a dual layer electrolyte, Mg as negative electrode and perovskite $BaTiO_3$ as positive electrode was tested at 55 °C by Sheha et al. [31]. The authors premagnesiated the perovskite $BaTiO_3$, heated the resulting Mg_xBaTiO_3 to 150 °C, and then it was used as a cathode in a Mg cell, with a capacity of around 68 mAh g^{-1}. The effect of magnesiation/heating at the perovskite was only on the surface to generate active sites that can adsorb/desorb Mg^{2+}. It was concluded that the electrochemical reactions mainly happen at the surface or near surface of the perovskite particles by means of a Mg-ion adsorption/desorption process, while the structure of the perovskite does not change. Another perovskite-type compound which has been tested for accommodation of magnesium is $Ba_{0.85}Sm_{0.1}TiO_3$. It has a tetragonal unit cell and ferroelectric properties. Soliman et al. found that only a small amount of magnesium (20 mAh g^{-1}) can be reversibly intercalated or adsorbed in this material even at 55 °C [32].

In this work, we have prepared titanate perovskites $A_xLa_yTiO_3$, with A = Li, Na and $(x+y) \leq 1$, and the electrochemical behavior as electrode active material for lithium, sodium and magnesium batteries has been studied. We discuss whether perovskite structure have available sites for electrochemical intercalation of lithium and post-lithium ions.

2. CALCULATIONS

DFT calculations were carried out in the frame of the GGA using the PBEsol correlation potential, as implemented in the CASTEP code [33], using a density-mixing scheme with a conjugate-gradient Pulay solver. The cut-off energy was fix at 600 eV. Spin polarized calculations were performed in all cases. For structure optimization we assumed that the host perovskite framework remains basically unchanged during the insertion and de-insertion processes, while the internal coordinates were optimized using the BFGS algorithm. The following convergence conditions were used: energy, 10^{-5} eV/atom; max. force, 0.03 eV $Å^{-1}$; max. stress, 0.05 GPa and max. displacement, 10^{-3} Å. The percolation energy has been calculated using soft-BVS/BVEL, as implemented in BondStr software.

3. EXPERIMENTAL

The lanthanum titanate samples LLTO and NLTO were prepared by the ceramic route. For LLTO, the reagents La_2O_3, TiO_2 and Li_2CO_3 weighed in the stoichiometry Li : La : Ti = 0.6 : 0.5 : 1 were firstly ground together in an agate mortar. The excess of lithium was used to compensate the loss during the synthesis. Then, the ground mixture was heated at 1250 °C for 12 h. For the synthesis of NLTO, La_2O_3, TiO_2 and $NaHCO_3$ were employed.

The crystalline structures of the samples were characterized by X-Ray Diffraction (XRD) using a Bruker D8 Discover A25 instrument with CuK_α radiation, Ge monochromator and

Lynxeye detector, from 10 to 90 °2θ, in steps of 0.04 and 3.5 s/step. The XRD patterns were fitted using the Rietveld method and Topas commercial software. Raman measurements were performed in a Jasco spectrophotometer. The particle morphology and composition were studied by Scanning Electron Microscopy (SEM) using a JEOL JSM 7800F apparatus

The electrochemical behavior was examined using Swagelok-type cells and a VMP instrument. The weight ratio of the working electrode was active material: polyvinylidene fluoride : carbon black = 80 : 10 :10. For lithium cell, a piece of Li was used as counter electrode, and the electrolyte solution was 1 M $LiPF_6$ in mixture of ethylenecarbonate (EC) and diethylcarbonate (DEC) (EC : DEC = 1 : 1). Counter: Li. I= 10 mA/g. For sodium cell, a piece of Na was used as counter electrode, and the electrolyte solution was 1 M $NaClO_4$ in PC containing 2% fluroethylenecarbonate (FEC). The electrochemical cells were ensembled in a M-Braun glove-box filled with Ar. The imposed current intensity was 10 mA g^{-1}. The ionic conductivities of the electrode materials were measured by using electrochemical impedance spectra [12].

4. RESULTS AND DISCUSSION

4.1.Structure of LLTO and NLTO

The XRD pattern of the obtained LLTO sample (Fig. 1A) can be indexed to the tetragonal perovskite-type structure and space group P4/mmm (n° 123), where c ≅ 2a (supercell 1x1x2), with a La-rich layer and a Li-rich layer [5, 7]. NLTO is described as a rhombohedral perovskite (s.g. $R\bar{3}c$, n° 167), where α ≅ 60 °) [11, 35-37], and where the occupancy of the layers is 50% La:50 % Na (fully disordered). Based on these models we have carried out the Rietveld refinements of the XRD patterns of LLTO and NLTO which results are included in Figure 1-A,B, and Tables 1, S1 and S2. We allowed La atoms to be located in all Li and La positions,

always keeping the stoichiometry of the compound. The refinement of LLTO confirms the presence of a partially disordered phase, with a layer containing 61 % of La atoms, and the other one 39 % of La atoms.

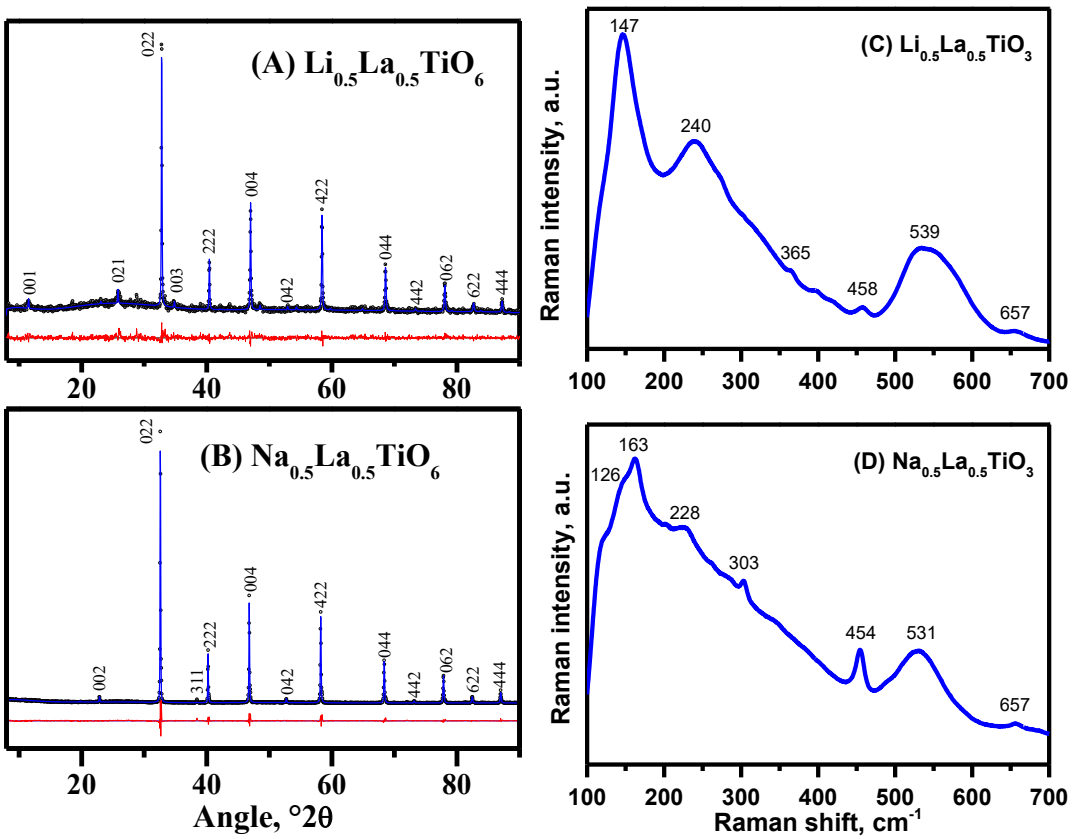

Figure 1. (A, B) XRD and Rietveld refinement and (C, D) Raman spectra for LLTO and NLTO.

The room temperature Raman spectra can be employed to obtain more insight into the local structure (Fig. 1C,D) [35-38]. It is expected that only vibrations of Ti and O atoms contribute to the bands, while La vibrations are not active. According to the literature, and within a tetragonal approach, the bands near 140 and 320 cm^{-1} are ascribed to in-plane and c-axis vibrations modes of titanium, respectively [38, 39]. All the other modes are assigned to oxygen vibrations. The ordering/disordering in the 1a and 1b sites affect to the narrowing/broadening of the Raman bands. For NLTO, the extra peaks and the broadening observed in the region 100-460 cm^{-1} can be attributable to a lower symmetry of NLTO structure compared to LLTO. The relative higher intensity of the peak at ca. 454 cm^{-1} is typical of the rhombohedral symmetry. Sanjuán et al. suggested that there are nanodomains of a quasi-tetragonal structure which would be embedded in the rhombohedrally arranged matrix [11].

According to the SEM micrographs, the morphology of the particles of NLTO is more globular, while the particles of LLTO tend to be more polyhedral. In addition, the size of the particles of NLTO is substantially smaller (around 100 nm) compared to LLTO (several micrometers) (Fig. 2), and in both cases the particles form aggregates of larger size.

Table 1. Selected refined parameter of LLTO and NLTO raw compounds. Details on Wyckoff sites are available in the S.I.

Compound	**$Li_{0.5}La_{0.5}TiO_3$**		**$Na_{0.5}La_{0.5}TiO_3$**	
Space Group	P4/mmm (123)	Pm$\bar{3}$m (221)	R$\bar{3}$c (167)	Pm$\bar{3}$m (221)
Z	1	4	3	4
Unit cell Parameters				
a / Å	3.8741(24)	7.7443 (39)	5.4779 (10)	7.7446 (19)
c / Å	7.7388(49)	---	13.4053 (29)	---
Vol / $Å^3$	116.15 (16)	464.46(70)	348.37 (15)	464.50 (44)
			Rhombohedral parameters	
a / Å			5.4739 (12)	5.4763 (13)
α / °			60.0420 (41)	60
Vol/Z / $Å^3$	116.15 (16)	116.12 (18)	116.088 (76)	116.13 (11)
Reliability Factors				
R_{wp}	18.59	18.60	17.41	17.06
R_{exp}	16.43	16.44	12.02	12.01
GoF	1.13	1.13	1.45	1.42
R_{Bragg}	2.05	1.74	2.79	2.89

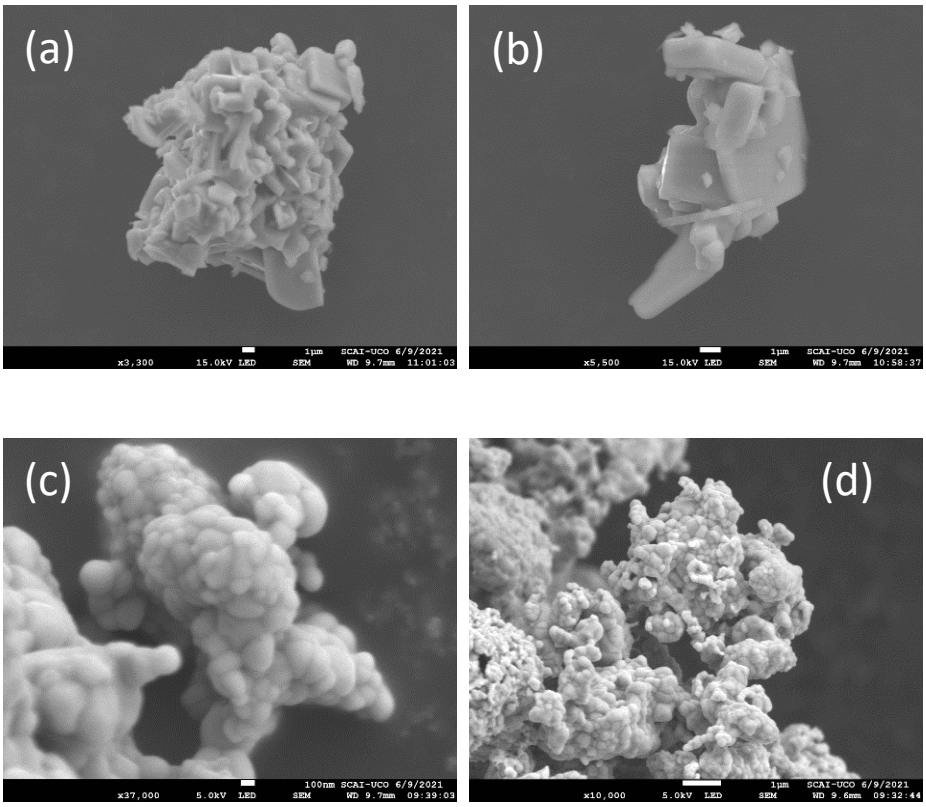

Figure 2. SEM micrographs for (a, b) LLTO and (c, d) NLTO.

4.2. Modeling LLTO and NLTO

We have optimized the theoretical structure of the perovskite-type LLTO and NLTO compounds by using DFT calculations. Based on the cubic unit cell of the perovskite, a 2x2x2 supercell was used. The different La/Li(Na) distributions used are schematized in Figure S1. In both (Li and Na) cases, the pseudo-layered structure (denoted as "Layer" in Figures 3 and S1 and Table S1) has the lower energy. This structure can be described as a framework formed by $[TiO_6]$ units, similar to ReO_3, being La and Li at the center of 8 octahedra, forming alternate

layers of Li and La (Fig. 3). However, the energy difference between the different configurations, especially with the “mix-lat” and “mix-diag” configurations, is relatively small (Table S1). These configurations can also be seen as layered phases, with a first layer 75 % La + 25 % Li and a second layer 25 % La + 75 % Li, where different ways of ordering cations are available, i.e. the atoms in the layers are somewhat disordered. This partial disorder can be favored by the high temperature of the synthesis, and the entropy term of this disordered configuration. This disorder has been already confirmed using Monte Carlo simulations by other authors [34].

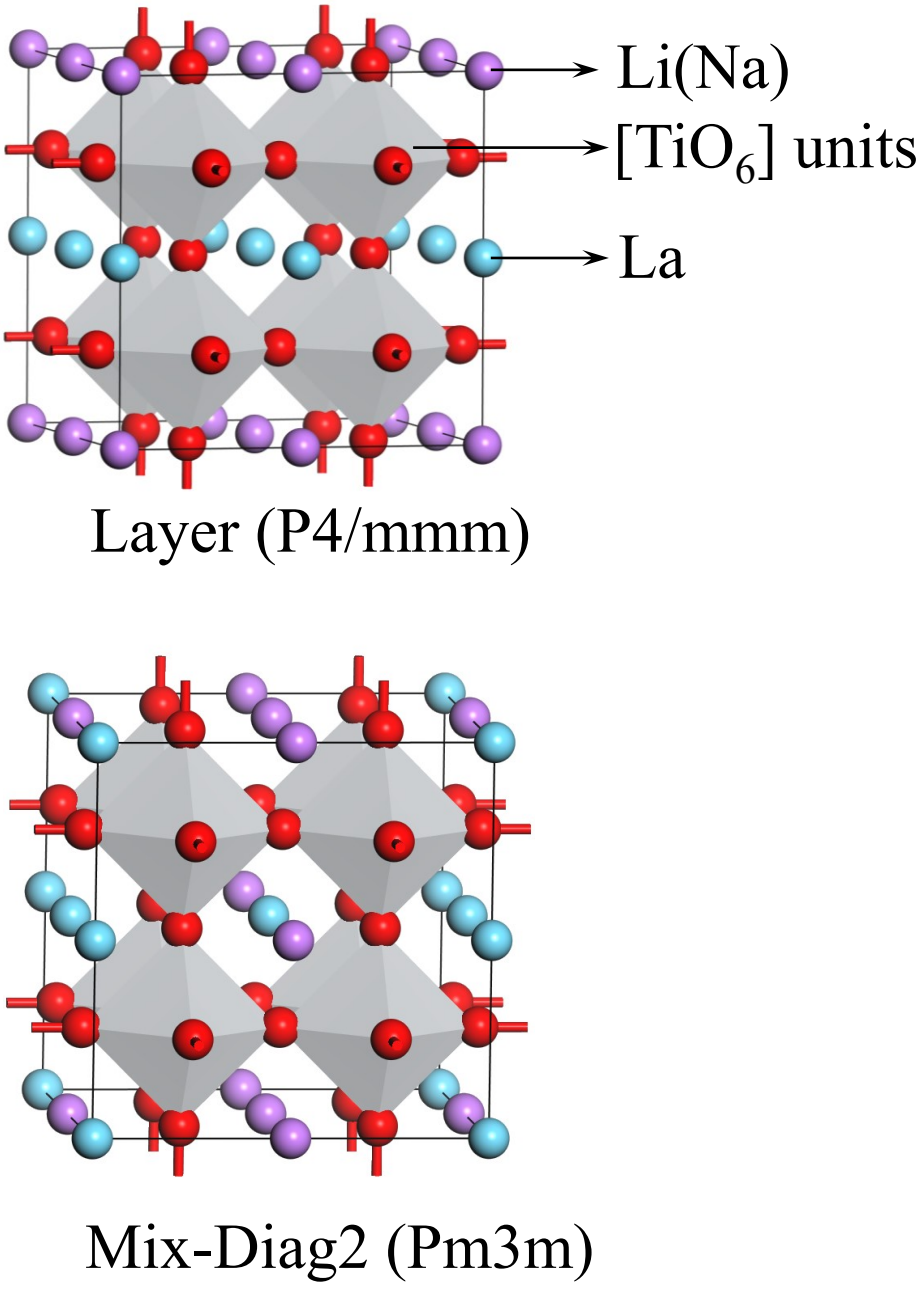

Figure 3. Main structural models used for DFT calculations.

It is also worth noting that the energy difference between the ordered (Layer) phase and these "disordered" phases (mix-lat and mix-diag, Figure S1) is ca. 82 meV in the case of Li, while in the case of Na is only 68 meV. Although small, this difference can justify why a higher disordered degree is obtained for NLTO than for the equivalent LLTO (see the structure description above). On the other hand, the site to accommodate La and Li(Na) atoms is large enough, and the calculated variations of volume for the different La/Li(Na) distributions are negligible. On increasing the temperature, the disorder can be expected to increase and finally reach a fully disordered system.

Alternatively, a model based on "MixDiag2" (Figure 3), with s.g. $Pm\bar{3}m$, was used to carried out the Rietveld refinements. The resulting quality of the refinement is like those using the previously proposed space groups (Table 1). After allowing exchange of Li(Na) and La atoms, the results show than in the case of NLTO the average occupancy of La in La-layer and Na-layers is 0.504 and 0.496, respectively, very close to the theoretical value 0.5 for the model based on the $R\bar{3}c$ space group. For LLTO the P4/mmm gives La occupancy values of 0.61 and 0.39, while when using $Pm\bar{3}m$ the occupancy is 0.57 and 0.43. The cell parameters calculated by DFT are also very close to those obtained from Rietveld analysis.

4.3. Modeling the insertion into LLTO and NLTO

At the light of the previous results on the structures of LLTO and NLTO, the calculations using the model based on "MixDiag2", with s.g. $Pm\bar{3}m$, can be used for studying the possible Li, Na and Mg insertion.

It has been proposed that there are three possible positions to intercalate lithium into the structure of the perovskite LLTO [18] (Fig. 4A): at the middle point of La-La, La-Li and Li-Li.

In all the three cases, Li is coordinated by 4 [TiO_6] units (Fig. 4B). Assuming that La^{3+} cations are not mobile species, the site La-La seems to be no available for insertion, as it is blocked by La atoms at both sides. Concerning the site La-Li, it will be opened on one side only, and can be regarded as a site for insertion (storage) but not for conductivity/diffusion. Finally, the full conductivity/diffusion is expected to use the Li-Li sites. The energy of the Li-insertion into these three sites has been calculated, based on a "MixDiag2" unit cell.

The Li insertion into the Li-Li site makes the neighboring Li atoms to be displaced from the center of their initial coordination site, as shown in Figure 4C. The displacement is somewhat important, ca. 0.085 fractional units, and neighboring Li approaches to the contiguous insertion sites, thus making difficult the insertion in those sites. An alternate filling along that direction is more probable, as shown in Fig. 4D, where the inserted Li are not equivalent to those present before insertion.

The insertion into the La-Li site strongly displaces the neighboring Li (ca. 0.120), while the inserted Li is also displaced from the center of starting position (ca. 0.084), so that both Li (already present before insertion and new inserted) becomes equivalent, as Figure 4E shows. On the contrary, La atoms are not affected. At the same time, [TiO_6] octahedra are somewhat tilted.

From the energy point of view this second option (La-Li site) is more stable, although the insertion in Li-Li site is only 0.047 eV higher in energy (Table 2). This Li insertion is expected at ca. 1.0 V vs. Li^+/Li. Finally, the insertion into La-La sites also makes the La neighbors to move away (ca. 0.049 eV), but the energy of such an insertion is greater than zero (and ca. 3.2 eV higher than in the other sites), and thus it can be discarded.

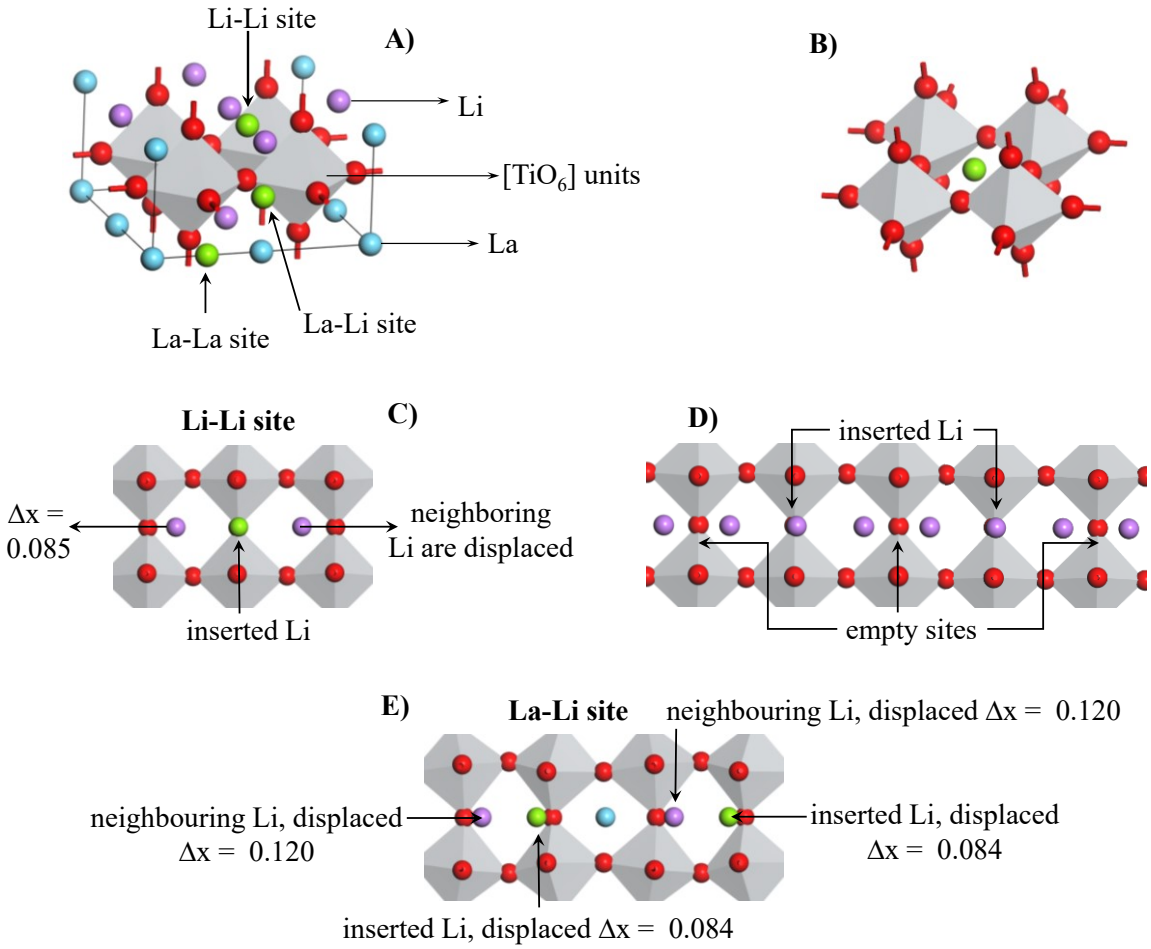

Figure 4. (A) Different positions for Li insertion: at the middle point of La-La, La-Li and Li-Li; (B) in the three cases the inserted ions are coordinated by 4 [TiO_6] units; (C) modifications after the Li insertion into the Li-Li site; (D) probable filling of insertion sites along a direction of Li-Li sites; (E) modifications after the Li insertion into the La-Li site.

Table 2. Calculated energy (in eV) of the different insertion sites for 1 Li, 1 Na and 1 Mg insertion into $Li_4La_4Ti_8O_{24}$ and $Na_4La_4Ti_8O_{24}$ supercell.

	Li insertion	**Na insertion**	**Mg insertion**
LLTO			
Li-Li site	– 0.95	– 0.46	+ 0.31
La-Li site	– 1.00	– 0.14	+ 0.55
La-La site	+ 2.21	---	---
NLTO			
Na-Na site	– 0.29	+1.12	+ 1.31
La-Na site	+0.08	+1.29	+ 1.89

To analyze the potential use of LLTO for Mg cells we also studied the theoretical insertion of Mg into Li-Li and Li-La sites. The size of Mg^{2+} is similar to that of Li^+ (0.72 Å and 0.76 Å, respectively), and one can expect to locate Mg cations in the same sites than those used for Li^+ insertion, although the higher repulsive interactions are expected with neighboring cations. For the Mg insertion into Li-Li sites, the neighboring Li atoms are also displaced (as it happens for Li insertion) ca. 0.120 fractional units. It is higher than in the case of Li insertion, probably due to the higher repulsions induced by Mg^{2+} as compared with Li^+. The insertion of Mg into La-Li site is also like that of Li, although the displacement of the Li atoms is again somewhat higher. Un fortunately, since the calculated variation of energy due to Mg^{2+} insertion in both cases is greater than zero (Table 2), the Mg-insertion is not thermodynamically expected to happen.

The insertion of Na into LLTO was also studied. The size of Na^+ (1.02 Å) is considerably larger than that of Li^+ and Mg^{2+}. Thus, when Na is inserted in a Li-Li site, Na is displaced close to the position of Li, while Li is displaced close to the other neighboring insertion position. A similar effect is observed when Na is inserted in a La-Li sites. The insertion in both sites is favorable from the energy point of view, although it is more stable in the Li-Li site. A comparison of the structural effects of Li, Na and Mg insertion in Li-Li and La-Li sites into LLTO is shown in Figure S2.

Finally, we also analyzed the insertion of Li, Na and Mg in Na-Na and La-Na sites into NLTO. As a conclusion for this analysis, only the insertion of Li into Na-Na site is favorable, with a negative value of the energy (– 0.29 eV, Table 2), although it is considerably smaller than the equivalent insertion into LLTO (– 0.95 eV). A moderate polarization during the Li insertion into NLTO experiment could make this insertion impossible. For all the other cases (inserted elements and sites) the insertion is not thermodynamically expected.

4.4. Electrochemistry of LLTO and NLTO in Li and Na cell

The perovskite LLTO shows a reversible capacity of ca. 140 mAh g^{-1} for the first cycle in lithium cell (Fig. 5A). This capacity value agrees well with previous studies [18] and with the reversible reduction of Ti^{4+} to Ti^{3+}. The capacity of the first discharge is larger (ca. 280 mAh g^{-1}) than the charge capacity, and this fact is due to the irreversible decomposition of the electrolyte solution and formation of a solid electrolyte interface, although we cannot discard that some lithium atoms intercalated during the first discharge remain irreversibly trapped in the framework of LLTO. The capacity is ca. 81 mAh g^{-1} over 100 cycles (Fig. 5B), and this result cell suggests that the structure is very stable. The composition of electrolyte solution could be optimized to increase the coulombic efficiency in the first 20 cycles. In contrast to lithium, the capacity in sodium cell is only ca. 10 mAh g^{-1} (Fig. 5C). These results evidence that the larger size of

sodium ion compared to lithium hinders the ionic mobility in the perovskite structure, and we can conclude that the replacement of lithium by sodium is not favorable, in good agreement with the theoretical calculations. After seeing the electrochemical results, most probably the electron content in the lattice of LLTO in sodium cell is not significantly modified, and the electrode material would be a poorer electronic conductor compared to LLTO lithium cell [13, 18]. The galvanostatic intermittent titration technique (GITT) was employed to obtain the diffusion coefficient of lithium in LLTO (Supplementary Fig. S3). The obtained values range from 10^{-10} to 10^{-8} cm^2s^{-1}(Fig. 5D), indicating a very good mobility of lithium in the perovskite structure, in good agreement with previous studies [18].

The specific capacity of the NLTO in lithium cell (Fig. 6A) is substantially lower (ca. 25 mAh g^{-1}) compared to LLTO. This low (or negligible) value of experimental capacity agrees well with the expected poor ionic mobility, and the La^{3+} ions in the tunnels forming a bottle neck for sodium mobility. It was experimentally checked that the conductive agent (carbon black) can contribute to the apparent capacity of the electrode (Fig. S4). In addition, the coulombic efficiency for the first cycle of NLTO in sodium cell (ca. 23%) is lower compared to lithium cell (ca. 47%) and, consequently, it seems that sodium atoms are irreversibly trapped in NLTO (Fig. 6B). Thus, it is concluded that it is impossible to replace sodium by lithium in NLTO by using these electrochemical cells. The ordered structure of the tetragonal perovskite-type LLTO and the relatively small size of lithium are the key factors that allow the intercalation of lithium into its framework, in contrast to NLTO. In addition, for NLTO and using impedance spectroscopy we obtained an ionic conductivity value $\sigma = 4{,}6 \times 10^{-6}$ S cm^{-1} at 24 °C, and this value is substantially lower than the values reported for LLTO in the literature [12]. On the contrary to the enhancement of the electronic conductivity after electrochemical insertion of Li into LLTO

due to the formation of Ti^{3+} [13, 18], it is expected that probably NLTO remains insulator in both lithium and sodium cell. For the sake of comparison of LLTO and NLTO, the diffusion coefficient of NLTO was also calculated from GITT curves in lithium cell (Supplementary Fig. S5). The values for NLTO (between $6x10^{-11}$ and $5x10^{-9}$ cm^2s^{-1}) are one order of magnitude lower than LLTO (Fig. 6C).

On the other hand, we tried to increase the capacity of the perovskite by creating ion vacancies through previous acid-treatment likely previous studies on other materials [40]. We thought that the cationic vacancies in the perovskite could improve the cationic mobility, similarly to manganese spinel [40] or, alternatively, the cationic exchange could modify the properties of the perovskite [41]. However, this procedure was not successful, the structure of the perovskite (LLTO and NLTO) was not modified even after five these in contact with nitric acid solution, and the experimental capacity was not significantly modified after acid treatment (not shown results). In fact, the results proved that the perovskite structure is very robust.

Table 3. Percolation energy of Li and Na into LLTO and NLTO, calculated for different structural models, depending on the structural disorder.

	Percolation energy / eV			
	Fully ordered: Layer model	**Partially disordered: mix-diag-2 model**	**From Rietveld refinement**	**Fully disordered model**
LLTO				
Li	0.26	0.35	2.99	4.26
Na	1.64	1.99	2.87	3.62
Mg	3.20	3.37	5.77	7.11
NLTO				
Li	1.98	2.05	2.00	
Na	2.25	2.18	1.96	
Mg	2.40	2.46	2.38	

To help understanding the kinetics of the cationic diffusion, we have calculated the percolation energy of the different A elements (Li, Na and Mg) in both LLTO and NLTO using different structural models. The calculated values are included in Table 3. The resulting values for lithium in LLTO using layered and mix-diag-2 models are especially low: 0.26 and 0.35 eV, respectively. Thus, this result confirms that ordered LLTO a very interesting material for lithium intercalation and diffusion. Figure 7 shows the isosurface corresponding to the Li percolation energy for the layered model. The Li mobility is restraint to Li planes, while diffusion perpendicular to Li-layers is fully blocked by La atoms. Unfortunately, on increasing the structural disorder the percolation energy strongly increases, up to reach more than 4 eV for the

fully disordered phase. Thus, a good ionic conductivity is expected only for phases with a high degree of Li/La layered ordering. This result confirms the importance of obtaining an ordered structure, playing with the synthesis conditions. A similar trend is observed for Na and Mg into LLTO, but in these cases even the values of the ordered phases are too high (1.64 and 3.20 eV, respectively) for expecting a practical ionic conductivity. Concerning NLTO, high values are obtained for all A elements and all structural models. This result agrees with the experimental measurement of the ionic conductivity of NLTO, as it is exposed above.

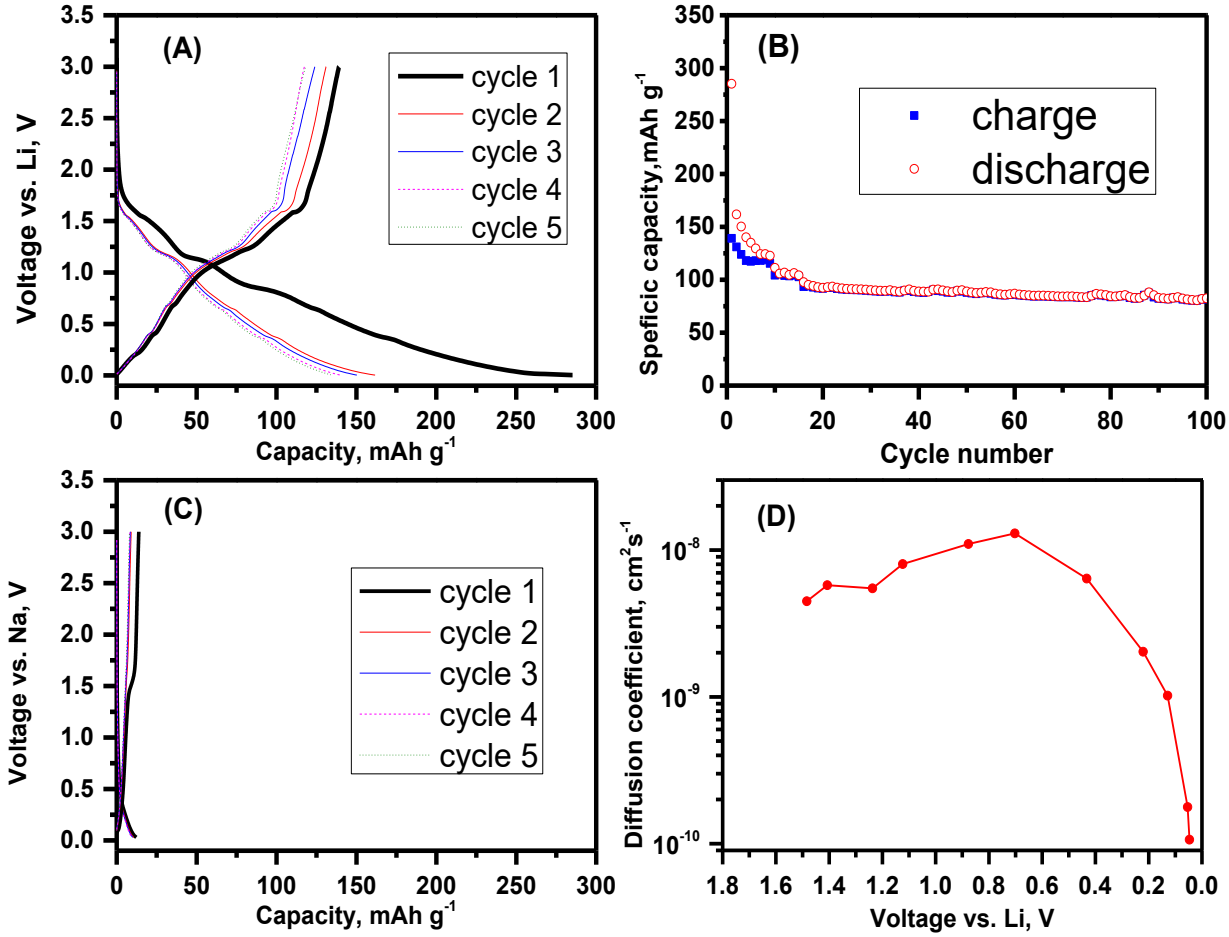

Figure 5. Electrochemistry of LLTO in (A, B) lithium and (C) sodium cell. (D) Lithium diffusion coefficient as a function of discharge voltage.

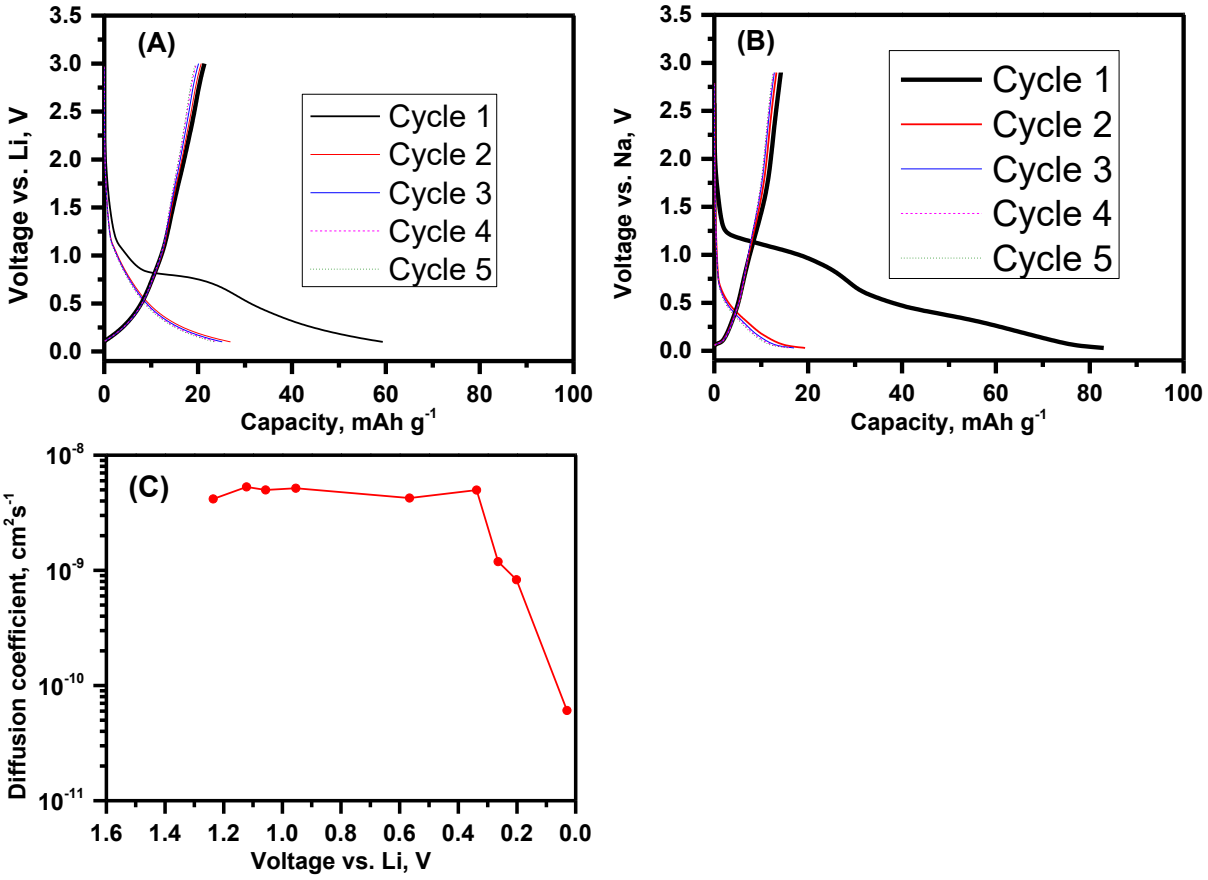

Figure 6. Electrochemistry of NLTO: (A) in lithium cell and (B) in sodium cell. (C) Diffusion coefficient as a function of discharge voltage obtained in lithium cell.

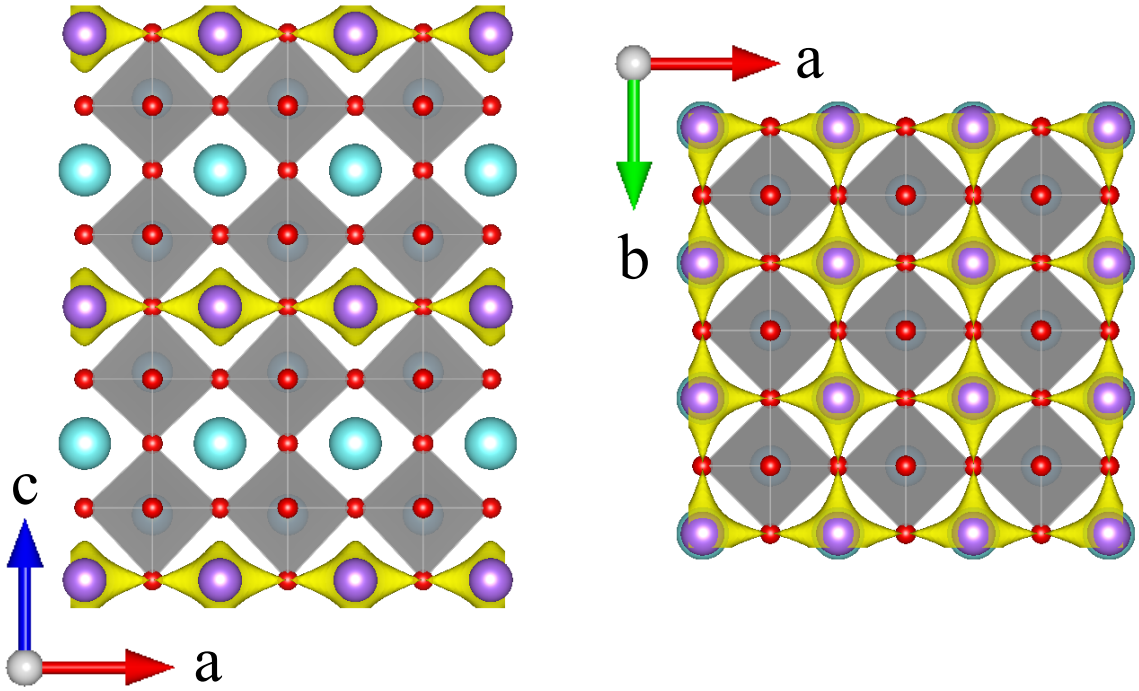

Figure 7. Projection of the ordered layered structure of LLTO, showing the isosurface at the Li percolation energy value. Color code: [TiO_6] units in grey; Li atoms in magenta; La atoms in blue; isosurface in yellow.

4.5.Electrochemistry of LLTO in Mg cell

Although Li^+ (r = 76 pm) and Mg^{2+} (r = 72 pm) possess nearly the same ionic radius, it is interesting to compare the effect of the charge in the experimental intercalation. The first discharge capacity of LLTO in magnesium cell is ca. 30 mAh g^{-1}, and this fact involves that the intercalation of Mg is very limited or negligible. On the contrary to the first discharge curve, the voltage-capacity curves (Fig. 8A,B) of the second and successive cycles exhibit endless plateaus at around 0.3-0.6 V vs. Mg. The charge-discharge plateaus and the hysteresis observed in the voltage curve cannot be ascribed to significant reversible (de)intercalation of magnesium in the

framework, and these are typical of side reactions at the particle surface (plateaus) or capacitive (surface) behavior. Similarly, Shesha et al and Soliman et al. reported reaction of Mg only at the particle surface for others perovskite-type compounds [31,32]. It could be that the perovskite catalyzes the decomposition of the electrolyte at the particle surface during the first discharge-charge cycle of LLTO, and then the surface properties and the voltage curve are modified for the successive cycles. The observed low capacity is in good agreement with the theoretical calculations on the insertion of naked magnesium into the structure of the perovskite LLTO. In addition, the electrochemical cycling of LLTO in magnesium cell was also carried out at 55 °C, to try to increase the capacity, but improvement was not observed (results not shown). The negligible capacity of the carbon black (without perovskite) in magnesium cell was also experimentally checked (Supplementary Fig. S6).

It is known that the traces of water in the liquid electrolyte solution can influence the electrochemical behavior of the batteries based on multivalent cations. The desolvation of Mg^{2+} from chelating molecules such as DME is not easy, and then the Mg-intercalation is difficult. The water molecules shielding the charge of Mg^{2+} could help to intercalate hydrated magnesium compared to naked (no shielded) magnesium, although the exact mechanism is still being investigated and protons could be intercalated [42-45]. Thus, to further study the behavior of LLTO in magnesium cell, electrochemical experiments were also performed using a wet electrolyte. For that purpose, the salt $Mg(TFSI)_2$ was used as received (not dried) and directly dissolved in DME. Thus, water is rather an additive, or an impurity, in this electrolyte. The discharge curves of the cycles 1-5 (Fig. 8C,D) are sloped, the endless plateau is not observed, and the reversible capacity is around 20-50 mAh g^{-1}, suggesting that there is a limited cationic intercalation even under these experimental conditions (wet electrolyte). This intercalation could be due to hydrated magnesium or protons [45], or even the apparent capacity could be due to

other side reactions. For example, the oxidative decomposition of TFSI can contribute to the pseudoplateau in the charge curve at ca. 3 V. In any case, the experimental results obtained under different conditions confirm the theoretical results about the unfavorable intercalation of Mg into the bulk of LLTO. However, we cannot discard the intercalation of Mg in other perovskite-type compounds and under different experimental conditions [46,47].

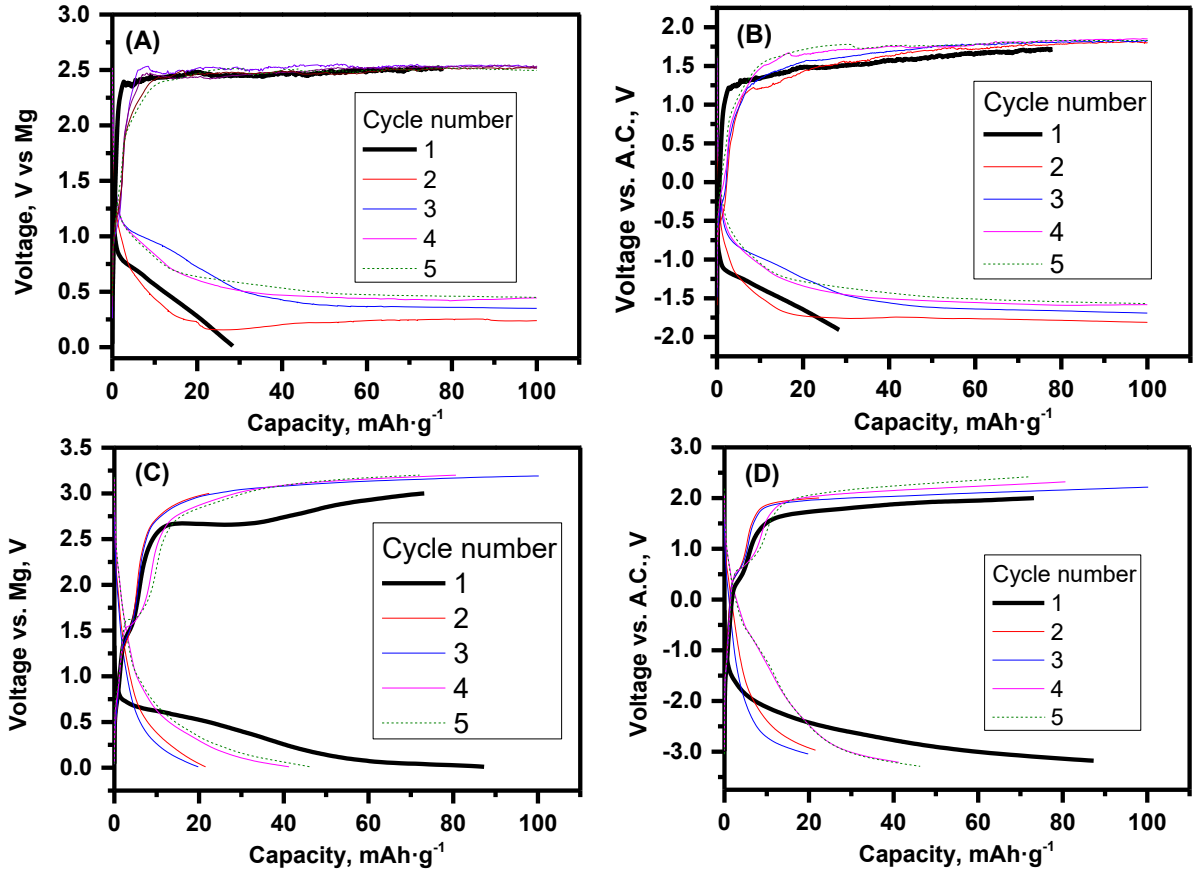

Figure 8. Electrochemistry of LLTO in three-electrode magnesium cell using (A, B) dry electrolyte, and (C, D) wet electrolyte.

5. CONCLUSION

The structure of the perovskite-type $Li_{0.5}La_{0.5}TiO_3$ is suitable for reversible lithium intercalation, and the maximum reversible capacity achieved here is ca. 150 mAh g^{-1}, while it cannot intercalate a decent amount of sodium. In contrast, the capacity of $Na_{0.5}La_{0.5}TiO_3$ is negligible in both lithium and sodium cell. The theoretical and experimental results conclude that the insertion and mobility of lithium into the stable perovskite structure is possible for many charge/discharge cycles, while the reversible insertion of sodium and magnesium are not feasible, and this is mainly due to the larger size of sodium ion compared to lithium, and to the charge of magnesium ion. The combination of theoretical calculations and experimental results can help to avoid misinterpretations of the electrochemical results and confusing side reactions with intercalation of multivalent ions, such as magnesium.

ASSOCIATED CONTENT

Supporting Information.

Details on: the structure models used in the theoretical calculations; calculated cell parameters and relative energy Li(Na)/La configurations; Wyckoff sites and coordinates of the Rietveld refinement; electrochemistry of carbon black in sodium and magnesium cell; GITT results.

AUTHOR INFORMATION

Corresponding Author

Ricardo Alcántara - *Department of Inorganic Chemistry and Chemical Engineering, Instituto Químico para la Energía y el Medioambiente (IQUEMA), Facultad de Ciencias, Universidad de Córdoba, Campus de Rabanales, Edificio Marie Curie, E-14071 Córdoba, Spain*;

orcid.org/0000-0002-6364-6728; Email: ralcantara@uco.es

Authors

Alejandro Medina - *Department of Inorganic Chemistry and Chemical Engineering, Instituto Químico para la Energía y el Medioambiente (IQUEMA), Facultad de Ciencias, Universidad de Córdoba, Campus de Rabanales, Edificio Marie Curie, E-14071 Córdoba, Spain*;

orcid.org/0000-0002-2737-5916

Carlos Pérez-Vicente - *Department of Inorganic Chemistry and Chemical Engineering, Instituto Químico para la Energía y el Medioambiente (IQUEMA), Facultad de Ciencias, Universidad de Córdoba, Campus de Rabanales, Edificio Marie Curie, E-14071 Córdoba, Spain*;

orcid.org/0000-0003-3507-3923

Author Contributions

R.A. conceived of the presented idea and wrote the manuscript. C.P.V. performed the calculations and wrote the manuscript. A.M. performed the laboratory experiments.

Funding Sources

RA and CP-V are indebted to *FEDER Junta de Andalucía* contract 1380025-R, and research group FQM288.

ACKNOWLEDGMENTS

We express thanks to SCAI-UCO (SEM and Raman) and the IUNAN for facilitating scientific instruments (XRD and XRF).

REFERENCES

1. Goel, P.; Sundriyal, S.; Shrivastav, V.; Mishra, S.; Dubal, D. O.; Kim, K. H.; Deep, A. Perovskite Materials as Superior and Powerful Platforms for Energy Conversion and Storage Applications. *Nano Energy* **2021**, *80*, 2411-2502, DOI: 10.1016/j.nanoen.2020.105552

2. Stramare, S.; Thangadurai, V.; Weppner, W. Lithium Lanthanum Titanates: A Review. *Chem. Mater*. **2003**, 15, 3974-3990, DOI: 10.1021/cm0300516

3. Zinkevich, T.; Schwarz, B.; Braun, P.; Weber, A.; Enrenberg, H.; Indris, S. Effect of Sintering Temperature on Li Diffusivity in $Li_{0.29}La_{0.57}TiO_3$: Local Hopping and Long-Range Transport. *Solid State Ion.* **2020**, 35, 115486, DOI: 10.1016/j.ssi.2020.115486

4. París, M. A.; León, C.; Santamaría, J.; Ibarra, J.; Várez. Li Mobility in the Orthorhombic $Li_{0.18}La_{0.61}TiO_3$ Perovskite Studied by NMR and Impedance Spectroscopies. *Chem. Mater.* **2000**, *12*, 1694-1701, DOI: 10.1021/cm9911159

5. Fourquet, J. L.; Duroy, H.; Crosnier-Lopez, M.P. Structural and Microstructural Studies of the Series $La_{2/3-x}Li_{3x}\square_{1/3-2x}TiO_3$. J. *Solid State Chem.* **1996**, *127*, 283–294 DOI: 10.1006/jssc.1996.0385

6. Yang, F. Z. T.; Peterson, V. K.; Schmid, S. Composition and Temperature Dependent Structural Investigation of the Perovskite-Type Sodium-Ion Solid Electrolyte Series $Na_{1/2-x}La_{1/2-x}Sr_{2x}ZrO_3$. *J. Alloys Compd.* **2021**, *863*, 158500, DOI: 10.1016/j.jallcom.2020.158500

7. Yang, K. -Y.; Wang, J. -W.; Fung, K. -Z. Roles of Lithium Ions and La/Li-Site Vacancies in Sinterability and Total Ionic Conduction Properties of Polycrystalline $Li_{3x}La_{2/3-x}TiO_3$ Solid Electrolytes ($0.21 \leq 3x \leq 0.50$). *J. Alloys Compd.* **2008**, *458*, 415–424, DOI: 10.1016/j.jallcom.2007.03.130

8. Sun, Y.; Guan, P.; Liu, Y.; Xu, H.; Li, S.; Chu, D. Recent Progress in Lithium Lanthanum Titanate Electrolyte Towards All Solid-State Lithium Ion Secondary Battery. *Crit. Rev. Solid State Mater. Sci*. **2019**, *44*, 265-282, DOI: 10.1080/10408436.2018.148555

9. Malkowski, T. F.; Sacci, R. L.; McAuliffe, R. D.; Acharya, S. R.; Cooper, V. R.; Dudney, N. J.; Veith, G. M. Role of Pairwise Reactions on the Synthesis of $Li_{0.3}La_{0.57}TiO_3$ and the Resulting Structure−Property Correlations. *Inorg. Chem.* **2021**, *60*, 14831−14843, DOI: 10.1021/acs.inorgchem.1c02136

10. Islam, Md. S.; Wang, S.; Nolan, A. M.; Mo, Y. First-Principles Computational Design and Discovery of Novel Double-Perovskite Proton Conductors. *Chem. Mater.* **2021**, *27*, 8278-8288, DOI: 10.1021/acs.chemmater.1c02432

11. Sanjuán, M .L.; Laguna, M. A.; Belous, A. G. V'yunov, O. I. On the Local Structure and Lithium Dynamics of $La_{0.5}(Li,Na)_{0.5}TiO_3$ Ionic Conductors. A Raman Study. *Chem. Mater.* **2005**, *17*, 5862-5866, DOI: 10.1021/cm0517770

12. Symington, A. R.; Molinari, M.; Dawson, J. A.; Statham, J. M.; Purton, J.; Canepa, P.; Parker, S. C. Elucidating the Nature of Grain Boundary Resistance in Lithium Lanthanum Titanate. *J. Mater. Chem. A* **2021**, *9*, 6487–6498, DOI: 10.1039/D0TA11539H.

13. Nakayama, M.; Usui, T.; Uchimoto, Y.; Wakihara, M.; Yamamoto, M. Changes in Electronic Structure upon Lithium Insertion into the A-Site Deficient Perovskite Type Oxides $(Li,La)TiO_3$. *J. Phys. Chem. B* **2005**, *109*, 4135-4143, DOI: 10.1021/jp046062j

14. García, M. F.; Fernández, N.; Borrego, K.; Martínez-Sarrión, M. -L.; Mestres, L. Herraiz, M. Study of the Lithium Insertion and De-insertion in Perovskite Praseodymium Bismuth Lithium Titanate. *J. Eur. Ceram. Soc.* **2005**, *25*, 729–734 DOI: 10.1016/j.jeurceramsoc.2004.01.019

15. Birke, P.; Scharner, S.; Huggings, R. A.; Weppner, W. Electrolytic Stability Limit and Rapid Lithium Insertion in the Fast-Ion Conducting $Li_{0.29}La_{0.57}TiO_3$ Perovkite-Type Compound. *J. Electrochem. Soc.* **1997**, *144*, L167–L169, DOI: 10.1149/1.1837713

16. Bohnke, O.; Bohnke, C.; Fourquet, J. L. Mechanism of Ionic Conduction and Electrochemical Intercalation of Lithium into the Perovskite Lanthanum Lithium Titanate. *Solid State Ion.* **1996**, *91*, 21–31, DOI: 10.1016/S0167-2738(96)00434-1

17. Shan, Y. -J.; Chen, L.; Inaguma, Y.; Itoh, M.; Nakamura, T. Oxide Cathode with Perovskite Structure for Rechargeable Lithium Batteries. *J. Power Sources* **1995**, *54*, 397–402, DOI: 10.1016/0378-7753(94)02110-O

18. Zhang, L.; Zhang, X.; Tian, G.; Zhang, Q.; Knapp, M.; Ehrenberg, H.; Chen, G.; Shen, Z.; Yang, G.; Gu, L.; Du, F. Lithium Lanthanum Titanate Perovskite as an Anode for Lithium Ion Batteries. *Nat. Commun.* **2020**, *11*, 3490, DOI: 10.1038/s41467-020-17233-1

19. Hua, C.; Fang, X.; Wang, Z.; Chen, L. Lithium Storage in Perovskite Lithium Lanthanum Titanate. *Electrochem. Commun.* **2013**, *32*, 5-8, DOI: 10.1016/j.elecom.2013.03.038

20. Xiong, X.; Yang, L.; Liang, G.; Wang, C.; Chen, G.; Yang, Z.; Che, R. A Low Strain A-Site Deficient Perovskite Lithium Lanthanum Niobate Anode for Superior Li^+ Storage. *Adv. Funct. Mater.* **2021**, *32*, 2106911, DOI: 10.1002/adfm.202106911

21. Fang, M.; Yao, X.; Li, W.; Li, Y.; Shui, M.; Shu, J. The Investigation of Lithium Doping Perovskite Oxide $LiMnO_3$ as Possible LIB Anode Material. *Ceram. Int.* **2018**, *44*, 8223-8231, DOI: 10.1016/j.jcis.2020.04.014

22. Chang, L.; Li, J.; Le, Z.; Nie, P.; Guo, Y.; Wang, H.; Xu, T.; Xue, X. Perovskite-Type $CaMnO_3$ Anode Material for Highly Efficient and Stable Lithium Ion Storage. *J. Colloid Interface Sci.* **2021**, *584*, 698-705, DOI: 10.1016/j.jcis.2020.04.014

23. Nguyen, A. T.; Phung, V.D.; Mittova, V.O.; Ngo, H. D.; Vo, T.N.; Thi, M. L. L.; Nguyen, V. H.; Mittova, I. Y.; Le, M. L. P.; Ahn, Y. N.; Kim, I. T.; Nguyen, T. L.

Fabricating Nanostructured $HoFeO_3$ Perovskite for Lithium-Ion Battery Anodes via Co-precipitation. *Scr. Mater.* **2022**, *207*, 114259, DOI: 10.1016/j.scriptamat.2021.114259

24. Wei, H. -X.; Huang, Y. -D.; Tang, L. -B.; Yan, C.; He, Z. -J.; Mao, J.; Dai, K.; Wu, X.-W.; Jiang, J. -B.; Zhang, J. -C. Lithium-Rich Manganese-Based Cathode Materials with Highly Stable Lattice and Surface Enabled by Perovskite-Type Phase-Compatible Layer. *Nano Energy* **2021**, *88*, 106288, DOI: 10.1016/j.nanoen.2021.106288

25. Lu, Z.; Ciucci, F. Anti-Perovskite Cathodes for Lithium Batteries. *J. Mater. Chem. A.* **2018**, *6*, 5185-5192, DOI: 10.1039/C7TA11074J

26. Lai, K. T.; Antonyshyn, I.; Prots, Y.; Valldor, M. . Extended Chemical Flexibility of Cubic Anti-Perovskite Lithium Battery Cathode Materials. *Inorg. Chem.* **2018**, *57*, 13296−13299, DOI: 10.1021/acs.inorgchem.8b01850

27. Kitajou, A.; Ishado, Y.; Yamashita, T.; Momida, H.; Oguchi, T.; Okada, S. Cathode Properties of Perovskite-type $NaMF_3$ (M = Fe, Mn, and Co) Prepared by Mechanical Ball Milling for Sodium-ion Battery. *Electrochim. Acta* **2017**, *245*, 424–429 DOI: 10.1016/j.electacta.2017.05.153

28. Bharathi, K. K.; Moorthy, B.; Dara, H. K.; Durai, L.; Kim, D. K. Electrochemical Properties of $Na_{0.5}Bi_{0.5}TiO_3$ Perovskite as an Anode Material for Sodium Ion Batteries. *J. Mater Sci*. **2019**, *54*, 13236–13246 DOI: 10.1007/s10853-019-03834-9

29. Arroyo-de Dompablo, M. E.; Krich, C.; Nava-Avenda–o, J.; Palacín, M. R.; Bard», F. In Quest of Cathode Materials for Ca Ion Batteries: the $CaMO_3$ perovskites (M = Mo,

Cr, Mn, Fe, Co, Ni). *Phys. Chem. Chem. Phys.* **2016**, *18*, 19966−19972. DOI: 10.1039/C6CP03381D

30. Chaupatnaik, A.; Barpanda, P. Perovskite Lead-Based Oxide Anodes for Rechargeable Batteries. *Electrochem. Commun*. **2021**, *127*, 107038 DOI: 10.1016/j.elecom.2021.107038

31. Sheha, E.; Liu, F.; Wang, T.; Farrag, M.; Liu, J.; Yacout, N.; Kebede, M. A.; Sharma, N.; Fan, L. -Z. Dual Polymer/Liquid Electrolyte with $BaTiO_3$ Electrode for Magnesium Batteries. *ACS Appl. Energy Mater.* **2020**, *3*, 5882−5892. DOI: 10.1021/acsaem.0c00810

32. Soliman, T. S.; Hessien, M. M.; Sheha, E. Probing a New Halogen-Free Electrolyte and $Ba_{0.85}Sm_{0.1}TiO_3$ Cathode for Mg Battery Applications. *J. Mater Sci. Mater. Electron*. **2021**, *32*, 28781-28791, DOI: 10.1007/s10854-021-07263-w

33. Clark, S. J.; Segall, M. D.; Pickard, C. J.; Hasnip, P. J., Probert, M. I. J.; Refson, K.; Payne, M. C. First Principles Methods Using CASTEP. *Z. Kristallogr.* **2005**, *220*, 567-570, DOI: 10.1524/zkri.220.5.567.65075

34. Symington, A. R.; Purton, J.; Statham, J.; Molinari, M.; Islam, M. S. Parker, S. C. Quantifying the Impact of Disorder on Li-Ion and Na-Ion Transport in Perovskite Titanate Solid Electrolytes for Solid-State Batteries. *J. Mater. Chem. A* **2020**, *8*, 19603-19611 DOI: 10.1039/D0TA05343K

35. Mitchell, R. H.; Liferovich, R. P. A Structural Study of the Perovskite Series $Na_{0.75}Ln_{0.25}Ti_{0.5}Nb_{0.5}O_3$. *J. Solid State Chem.*, **2005**, *178*, 2586-2593 DOI: 10.1016/j.jssc.2005.05.016

36. Ranjan, R.; Senyshyn, A.; Boysen, H.; Baehtz, C.; Frey, F. Crystal Structures of $Na_{1/2}Ln_{1/2}TiO_3$ (Ln: La, Eu, Tb). *J. Solid State Chem.* **2007**, *180*, 995–1001. DOI: 10.1016/j.jssc.2006.12.030

37. Garg, R.; Senyshyn, A.; Boysen, H.; Ranjan, R. Structure and Phase Transition of $Na_{0.5}La_{0.5}TiO_3$. *J. Phys. Condens. Matter.* **2008**, *20*, 505215. DOI: 10.1088/0953-8984/20/50/505215

38. Sanjuán, M. L.; Laguna, M. A. Raman Study of Antiferroelectric Instability in $La_{(2-x)/3}Li_xTiO_3$ ($0.1 \leq x \leq 0.5$) Double Perovskites. *Phys. Rev. B* **2001,** *64*, 174305. DOI: 10.1103/PhysRevB.64.174305

39. Sanjuán, M. L.; Laguna, M. A.; Várez, A. Sanz, J. Effect of Quenching on Structure and Antiferroelectric Instability of $La_{(2-x)/3}Li_xTiO_3$ Compounds: a Raman Study. *J. Eur. Ceram. Soc.* **2004**, *24*, 1135–1139 DOI: 10.1016/S0955-2219(03)00581-8

40. Medina, A.; Rodríguez, A. I.; Pérez-Vicente, C.; R. Alcántara. Testing the Reversible Insertion of Magnesium in a Cation-Deficient Manganese Oxy-Spinel through a Concentration Cell. *Dalton Trans.* **2021**, *50*, 2123-2130, DOI: 10.1039/d0dt03856c

41. Boulant, A.; Bardeau, J. F.: Jouanneaux, A.; Emery, J.; Buzare, J.-Y.; Bohnke, O. Reaction Mechanism of $Li_{0.30}La_{0.57}TiO_3$ Powder with Ambient Air: H^+/Li^+ Exchange

with Water and Li_2CO_3 Formation. *Dalton Trans.* **2010**, *39*, 3968-3975, DOI: 10.1039/b924684c

42. Yoo, H. D.; Jokisaari, J. R.; Yu, Y. -S.; Kwon, B. J.; Hu, L.; Kim, S.; Han, S. -D.; Lopez, M.; Lapidus, S. H.; Nolis, G. M.; Ingram, B. J.; Bolotin, I.; Ahmed, S.; Klie, R. F.; Vaughey, J. T.; Fister, T. T.; Cabana, J. Intercalation of Magnesium into a Layered Vanadium Oxide with High Capacity. *ACS Energy Lett.* **2019**, *4*, 1528–1534, DOI: 10.1021/acsenergylett.9b00788

43. Medina, A.; Cabello, M.; Alcántara, R.; Pérez-Vicente, C.; Tirado, J. L. Theoretical and Experimental Study on the Electrochemical Behavior of Beta-Sodium Vanadate in Rechargeable Magnesium Batteries Using Several Electrolyte Solutions. *J. Electrochem. Soc.* **2020**, *167*, 070512, DOI: 10.1149/1945-7111/ab68d5

44. Spahr, M.E.; Novák, P.; Haas, O.; Nesper, R. Electrochemical Insertion of Lithium, Sodium, and Magnesium in Molybdenum(VI) oxide. *J. Power Sources* **1995**, *54*, 346–351, DOI: 0.1016/0378-7753(94)02099-O

45. Park, M. J.; Asl, H. Y.; Manthiram, A. Multivalent-Ion versus Proton Insertion into Battery Electrodes. *ACS Energy Lett.* **2020**, *5*, 2367−2375, DOI: 10.1021/acsenergylett.0c01021

46. Sheha, E.; Kamar, E. M.; Fan, L. -Z. Study the Structure and Electrochemical Performance of $BaTiO_3$/S Electrode Material for Magnesium-Ion Batteries. *Mater. Lett*. **2021**, *284*, 129033, DOI: 0.1016/j.matlet.2020.129033

47. Yacout, N.; Refai, H. S.; Kebede, M. A.; Salman, F.; Sheha, E. Significant Study of $BaTiO_3$ as Cathode for Magnesium Battery Applications. *Mat. Chem. Phys.* **2022**, *292*, 126770, DOI: 10.1016/j.matchemphys.2022.126770

Graphic for manuscript (For Table of Contents Only)